


Comparison of neural networks based on accuracy and robustness in identifying impact location for structural health monitoring applications

Structural Health Monitoring
2023, Vol. 22(1) 417–432
© The Author(s) 2022
Article reuse guidelines:
sagepub.com/journals-permissions
DOI: 10.1177/14759217221098569
journals.sagepub.com/home/shm


Prabakaran Balasubramanian¹ , Vikram Kaushik¹, Sumaya Y Altamimi¹, Marco Amabili^{1,2} and Mohamed Alteneiji¹

Abstract

Structural health monitoring systems must provide accuracy and robustness in predicting the structure's health using the minimum intervention to ensure commercial viability. Characterization of impact is useful in assessing its severity, deciding if detailed damage analysis is necessary, and re-evaluating the present health of the structure under monitoring with better confidence. In this characterization process, the impact location is significant since some positions within a structure are more sensitive to damage. The inherent noise and uncertainties present in the sensor response pose a substantial hurdle to estimating the external impact correctly. This paper quantitatively compares three of the widely used neural networks, namely, Artificial Neural Network (ANN), Convolutional Neural Network (CNN), and Long Short-Term Memory network (LSTM), to estimate impact location from the lead zirconate titanate (PZT) sensor response. For this purpose, a square aluminum plate of 500 × 500 mm was equipped with four PZT sensors; each placed 100 mm away in both the plate directions from a corner and impact loads were given on a grid covering the whole plate. The PZT responses were used to train the three neural networks under study here, and their estimations were compared based on the Mean Absolute Error (MAE). In addition, increasing Gaussian noise was added to the PZT responses, and the robustness of the three neural networks was monitored. It was found that the ANN gives better accuracy with a Mean Absolute Error of 22 mm compared to Convolutional Neural Network (MAE = 31 mm) and Long Short-Term Memory (MAE = 25 mm). However, CNN is more robust when encountering noise with a 2% reduction in accuracy, while LSTM and ANN lost 7% and 11% accuracy, respectively.

Keywords

Supervised machine learning, structural health monitoring, impact location identification, Artificial Neural Network, Convolutional Neural Network, Long Short-Term Memory network, robustness, accuracy

Introduction

Structural health monitoring (SHM) is a term used for continuous real-time inspection of structures for diagnosis and prognosis purposes. The diagnosis aspects covered by SHM systems include any changes in the current state of the structure that might affect the intended performance compared to its original state. The changes in the structure can be as broad as material or geometric property and boundary condition changes. The changes can also be the location of the newly developed crack, delamination, external impact, and their severity. Prognosis SHM systems provide information about the remaining life of the structure, given its current state of the structure. Both the diagnostic and

prognostics SHM systems use either independent or common sensor networks placed at strategic locations of the structure. SHM has been at the forefront of intensive research for the past few decades due to its strong economic and safety

¹Advanced Material Research Center, Technology Innovation Institute, Abu Dhabi, UAE

²McGill University, Montreal, QC, Canada

Corresponding author:

Prabakaran Balasubramanian, Advanced Material Research Center, Technology Innovation Institute, P.O. Box 9639, Masdar City, Abu Dhabi, UAE.

Email: prabakaran.balasubramanian@tii.ae

motivations in the areas of, including but not limited to, aerospace,¹ nuclear,² civil,³ and space.^{4,5} SHM research took a paradigm shift in the early 2000s towards statistical pattern recognition^{6,7} approaches for all aspects of SHM system development. Even though there has been a significant contribution from the research community,^{7–10} commercial implementation of SHM is still not widespread. Reliability of sensors,¹¹ the robustness of the diagnostic/prognostic algorithms during operational and environmental loads,¹² funding the technology to commercial maturity,¹³ inability to have all possible experimental damage scenarios, computationally expensive simulation,^{7,14} and validation of simulation models for various realistic damages^{7,14} are some of the issues hindering/preventing the commercial success of SHM.

Artificial Neural Networks (ANNs) and other Machine Learning (ML) approaches are some of the widely used statistical pattern recognition approaches in the SHM research.^{15–17} Neural networks are essentially a collection of artificial neurons, similar to the biological neurons in the human brain, arranged in the form of a network from input array to output array.^{18,19} Neural networks rose to fame again after the advent of low-cost graphical processing units and the availability of a large amount of data.^{20,21} Various branches of neural networks were developed to address specific downfalls of conventional neural networks.^{21–23} A neural network containing one or more hidden (neurons placed in between the input and output array) layers is called a deep neural network, which is one of the branches of neural networks. It is shown that with a sufficient number of hidden layers and nonlinear activation functions, deep neural networks can be a universal approximator.^{7,24,25} A comprehensive review of damage detection and identification based on vibration response using ANN was given by Gomes, G.F., et al.²⁶ ANNs were successfully used for damage detection and localization on an aluminum beam²⁷ and composite plates.²⁸ Even complex damages in composite plates, such as fatigue matrix cracking and delamination, were localized and identified by well-trained ANNs.²⁹ Early works of impact location detection using neural work dates back to the 2000 s.^{30,31} Impact location identification is a regression problem, where the output (x and y coordinate of the impact) is a continuous variable, and understandably ANNs were modeled accordingly. It is important to note that ANNs need salient features to be extracted from the time or frequency domain data to be efficient. Many scholars demonstrated external impacts localization and quantification using neural networks on various structures with varying accuracy depending on the feature extraction method, number, and type of sensors and the architecture of neural networks.^{32–36}

Convolutional Neural Network (CNN) uses convolution operation to learn global patterns and is the de facto standard for image recognition problems such as self-driving, object classification, or facial recognition.^{37–39} Traditionally,

CNNs are used for image recognition purposes. However, they are quite valuable for time-domain data as well,⁴⁰ such as electrocardiogram signal classification,⁴¹ fault detection in power engines,⁴² and much more. In contrast to ANN, CNN does not need the relevant features extracted from the time-domain data to work effectively. Thus, CNNs do not require an effective feature extraction process or pre-processing of the data. CNNs are very good at generalizing the problem and identifying the inherent patterns present in the input signal, which could be used to map the input with output. These patterns are somewhat tolerant of environmental effects such as noise.⁴³ One-dimensional CNNs have made significant contributions in damage^{44,45} and impact detection⁴⁶ of various structures. Gulgec, N.S., et al.⁴⁷ used CNNs to accurately detect and localize damages in civil structures from the raw strain field measurements. CNNs were combined with Naïve Bayes to produce significantly better crack detection systems in nuclear power plant components.⁴⁸ Strain data from an aircraft wing due to aerodynamic loads were given as an input to CNNs to localize damages by Lin, M., et al.,⁴⁹ where the noise-tolerant property of CNNs was effective. Typically, when CNNs are used for impact localization purposes, the problem is treated as a classification problem,⁴⁶ where the output is the probability of a particular impact belonging to a specific class or area, rather than a regression problem. Since the ANNs and CNNs are treating the impact location identification fundamentally differently, there are no studies on the measurable benefits of one over the other. A thorough review of CNNs in structural health monitoring applications in civil engineering is given by Sony, S., et al.⁵⁰

Almost all SHM systems rely on some form of sensor's responses to give diagnostic/prognostic results about the structure under observation. The sensor responses are a series of values concerning time; thereby, an inherent relationship is present between the values. ANN and CNN fail to consider these relationships and treat the data as independent. Recurrent Neural Networks (RNNs) address this downfall by creating a memory unit that relates the output with the history of inputs. RNN is also a featureless neural network similar to CNN. The difference between the structure of the RNN and the typical artificial neuron is that it has a recursive structure, which can transfer the information from the last state to the current state. Long Short-Term Memory (LSTM) is an advanced RNN technique that can remember history for a long time. The time-sensitive nature of RNN was used for impact diagnosis in stiffened structural panels using a deep learning approach RNN and CNN.⁵¹ The LSTM network was used to monitor the health of automobile suspension.⁵² However, to the knowledge of the authors, LSTM was not used to localize the impacts in the context of SHM.

Even though numerous neural networks cater to various aspects of SHM systems, there is very little work on their

effectiveness against temperature or humidity changes, environmental or operational loads/influences. The uncertainties were considered in developing ANN in the early work of Bakhary, N., et al.⁵³ The environmental and operational conditions were considered for the impact localization study by Seno, A. H., and Aliabadi, M.⁵⁴ The effect of noise was considered in developing a robust CNN called SHNnet by Zhang, T., et al.⁵⁵

Identifying the location of external impact is essential for SHM systems to understand its severity and subsequently predict the current state of the structure. This paper compares three commonly used neural networks (ANN, CNN, and LSTM) for their accuracy and robustness in identifying the impact location from lead zirconate titanate (PZT) sensor responses using a common metric. For this purpose, an aluminum plate was manufactured and instrumented with four PZT sensors. The PZT impact responses were given as input to train and compare these networks. The effect of environmental noise on the robustness of these neural networks was given less attention in the literature, according to the knowledge of the authors. Hence, each of these networks' robustness in the presence of added Gaussian noise, representative of environmental loads such as aerodynamic pressure, wind disturbance, and electrical noise, is also studied.

Method

Experimental setup

An aluminum plate (6061-T6) with the dimension of $500 \times 500 \times 2$ mm was manufactured from commercially available aluminum sheets of thickness 2 mm. The plate was instrumented with four PZT (PZT-5A, 10 mm diameter, and 2 mm thickness) sensors, as shown in Figure 1. Each PZT sensor was placed 100×100 mm away from a corner of the plate. The top left PZT sensor is named S1, the top right is labeled S2, the bottom left is S3, and the bottom right is S4. The center of the S1 sensor was chosen as the origin (o) of the coordinate system. The assumed x and y axes are depicted in Figure 1. The PZT sensors were glued to the plate using epoxy glue (Araldite) to ensure adequate bonding and energy transfer between the sensors and the plate. The electrodes of the PZT sensors were soldered to wires and connected to an oscilloscope (Teledyne T3DSO1204) through coaxial cables for data acquisition. The sampling rate was chosen to be 250 MSamples/sec. The response of the PZT sensor S1 was selected as the trigger channel to measure the impact response from all four sensors. A trigger value of 0.1 V and a pre-trigger duration of 1400 microseconds were set. The selected trigger value and pre-trigger duration were appropriate to ensure accurate impact response measurements while ignoring the false trigger due to the inherent electrical noise in the circuit. The total time

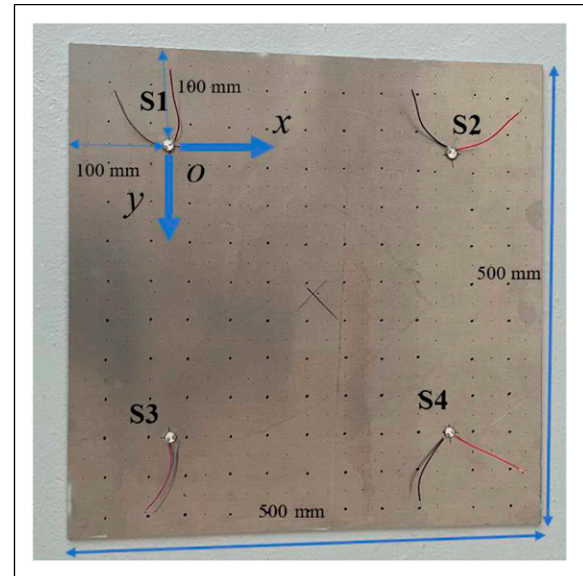


Figure 1. The aluminum plate with PZT sensors.

window of measurement was 0.14 s leading to 35 MSamples for every measurement. The oscilloscope was directly connected to a personal computer (PC) using a USB cable for storing the impact responses after every impact.

The plate was divided by a $40 \text{ mm} \times 40 \text{ mm}$ grid, represented by the black dots in Figure 1. A permanent marker was used for marking purposes after careful measurement. One column was left out as it was close to S2 and S4. The grid has 12 rows and 11 columns, resulting in 132 (12×11) grid points. An impact hammer produced the impact (Brüel & Kjær type 8204) attached with a metal tip. Erasable ink was used at the tip of the impact hammer before every impact to measure the impact location accurately. If the impact was more than ± 2 mm away from the grid point, the impact was ignored, thus ensuring repeatability of the impacts. The impact response data was measured from the four PZTs and stored.

Artificial Neural Network

The artificial neuron on which the neural networks are based is shown in Figure 2. The neuron receives a set of inputs (in this explained case, x_1 and x_2 , refer to Figure 2) and produces a single output, y . The weights are randomly selected and then optimized to reduce the error between the desired y and the predicted y . The error is sent backward from the output layer to the consecutive layers until it reaches the input layer while adjusting the weights. This approach is called backpropagation, and it was a significant step in making neural networks such a powerful method.⁵⁶ It is important to note that y is a function of z (weighted sum of inputs), typically known as an activation function. The

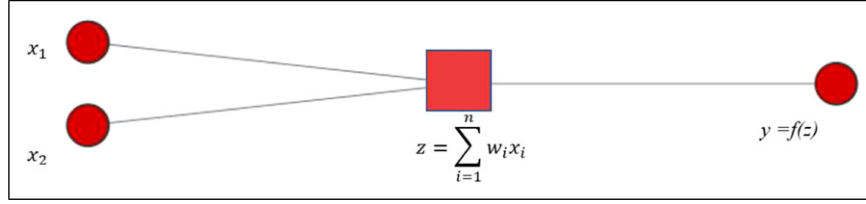


Figure 2. The artificial neuron.

activation function can be linear or nonlinear. Typical activation functions include but are not limited to ReLU, Leaky ReLU, softmax, sigmoid, Tanh, and linear.¹⁸ More detailed information on neural networks and deep learning can be found in the literature.^{18,57}

Pre-processing of the data for Artificial Neural Network. The responses are high-dimensional data, and directly using them to train an ANN would lead to under/overfitting. Under/overfitted ANN fails to generalize the impact location identification problem. Hence, pre-processing of the data is required to extract features that are appropriate for impact location identification. Time of Flight (TOF) and energy were chosen as the two salient features for the ANN developed here. The TOF is when the impact response arrives at the PZT location from the time of impact. The TOF is estimated by calculating the Akaike Information Criterion (AIC). The impact response signal from PZT can be divided into two segments; the segment before (majorly the noise) and after (dominated by the impact signal) the impact response arrives. Since the two segments are stochastically different, the best possible fit is achieved when the signal is divided strictly at the TOF. The AIC^{58,59} measures the quality of fit between several statistical models for a given dataset. By dividing the dataset at various separation points along the length of the signal and calculating AIC for both the datasets, we could find the time at which the AIC value was minimum. The time at which AIC is minimum corresponds to the TOF. The AIC of the impact response signal v at time t with a total length L can be calculated by^{54,60}

$$AIC(t) = t \ln(\text{var}(v_{1 \text{ to } t})) + (L - t - 1) \ln(\text{var}(v_{t+1 \text{ to } L})) \quad (1)$$

where $v_{1 \text{ to } t}$ is the segment of the signal up to the time t , $v_{t+1 \text{ to } L}$ is the rest of the signal, and $\text{var}()$ is the variance of the dataset. Similarly, the energy of the signal can be calculated as

$$E = \sum_{i=0}^T |v(t_i)|^2 \quad (2)$$

It is important to note that all four PZT sensors will have a unique sensitivity value, much like a typical sensor, due to variations in manufacturing and installation (gluing and soldering). Due to this sensitivity value, the response from

each PZT sensor is different in magnitude for the same impact from the same distance. However, the TOF is the same as it does not depend on the sensitivity. A simple calibration routine was introduced to estimate the correction factors by recording the response from all four PZTs due to an identical impact. Before estimating TOF and energy, the estimated correction factor was applied to all four PZT responses.

Artificial Neural Network architecture

The TOF and energy of four sensors because of impact were taken as input for ANN. The TOF and energy of the sensors were calculated based on the procedure explained in the previous section. The input data matrix is 132 (total number of impacts) \times 8 (4 sensors with 2 features each), referred to as X . The output matrix is 132 (total number of impact) \times 2 (x and y coordinates of the impact), referred to as Y . The data matrix is randomly divided into training, validation, and testing datasets with a 70/15/15 ratio split, respectively. The validation and testing dataset are essential to ensure that the model is not overfitting the training dataset. If the neural network model overfits the training data, the validation and testing data accuracy will be much lower than the training accuracy. The model's accuracy in the testing dataset will be considered the actual accuracy of the model.

The proposed architecture of the ANN consists of an input layer with eight nodes, followed by two hidden layers, each with a node size of 128. Finally, the output layer with two nodes representing the x and y coordinates of the impact. The ANN architecture is sketched and shown in Figure 3 with the help of an online tool.⁶¹ The ReLU nonlinear activation function was chosen between the first three layers, while the linear activation function was selected between the third and output layer. *Adams* optimization algorithm⁶² was selected for optimizing the model's weights as it adopts the learning rate according to the problem. The network was trained for 2500 epochs, and the validation dataset was used to verify the accuracy model. The error/loss is defined as the Mean Absolute Error (MAE) between the true and predicted impact location values

$$MAE = \frac{\sum_{i=1}^n |Y_{pred} - Y_{true}|}{n} \quad (3)$$

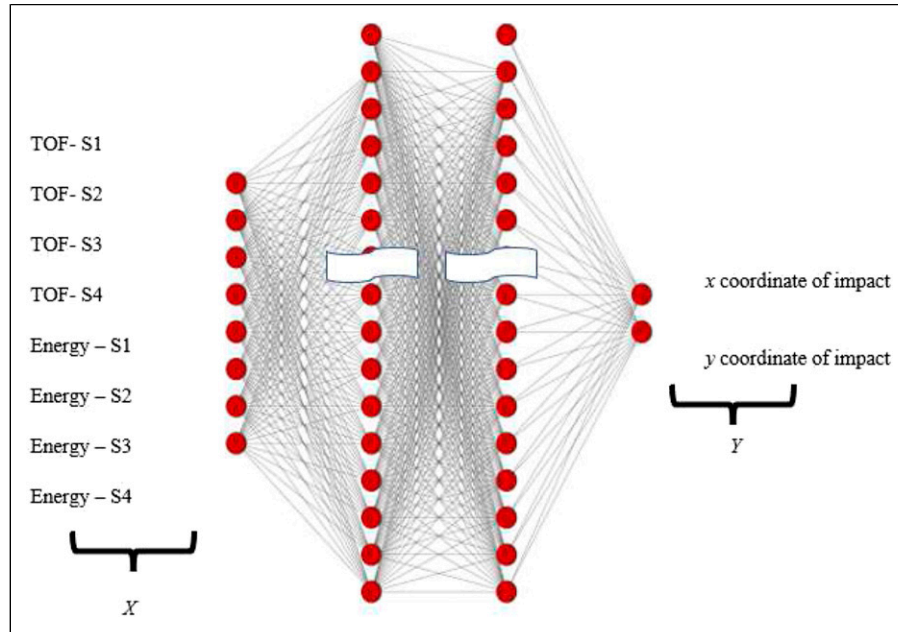


Figure 3. The proposed Artificial Neural Network architecture.

where Y_{pred} is the predicted location (x, y) of the impact, Y_{true} is the true location of the impact, and n is the total number of impacts.

Convolutional Neural Network

In contrast to ANN, CNN does not need salient features extracted from the PZT sensor response for impact location identification. The building blocks of typical CNNs are the convolution, pooling, and fully connected layers. The convolution layer is the first layer in any CNN and uses several convolution kernels to build feature representations of the input. There can be more than one convolution layer in a single CNN, and each layer builds the feature maps with increasing complexity. For example, the first convolution layer would learn to identify slopes and flat lines from time-domain data, while the second layer would build simple shapes from the previously identified slopes and flat lines. Finally, the third convolution layer might construct the relationship between slopes of two different time-domain signals. As the number of convolution layers increases, the ability of the model to cover a wider area of the image increases along with the computational burden. Detailed information on each of these layers and how they can be used to construct a fully functional CNN can be found in Refs. 18, 63, 64.

The following CNN architecture was used in this paper for impact location identification and is presented in Figure 4. The time-domain signal from all 4 PZT sensors is downsampled and converted into a matrix of 2000×4 (marked as 1 in Figure 4). The matrix is passed through five

consecutive layers (marked as 2 to 6 in Figure 4) of convolution and max pooling layers to reach the matrix size of $125 \times 1 \times 128$. The kernels are 3×3 size, and the *same* padding was used for convolution layers, while a kernel of 3×3 size and strides size of 2 with the *same* padding was used for the max pooling layers. The output from the final convolution and max pooling layer is flattened (marked as 7 in Figure 4), and size is reduced subsequently through a dense hidden layer (marked as 8) to an output of 2×1 matrix. The output corresponds to the x and y coordinates of the impact location. Similar to the ANN, the 132 impacts were split with a 70/15/15 ratio for training, validation, and testing purposes.

Long Short-Term Memory network

Long Short-Term Memory network is also a featureless neural network where there is no need to carefully extract the relevant features and feed them to the network to get acceptable accuracy. The time-domain data from the PZT sensors can be directly provided to the neural network, and the network automatically learns the relevant features. A single LSTM unit comprises a cell, an input gate, an output gate, and a forget gate. The cell remembers the values over arbitrary time intervals and the three gates regulate the flow of information into and out of the cell. Multiple LSTM units are typically connected in series and parallel to create a single LSTM network.⁶⁴ The LSTM network architecture chosen for the problem under study here is given in Figure 5. The response from all four PZT sensors was downsampled and stacked together as an input to the LSTM

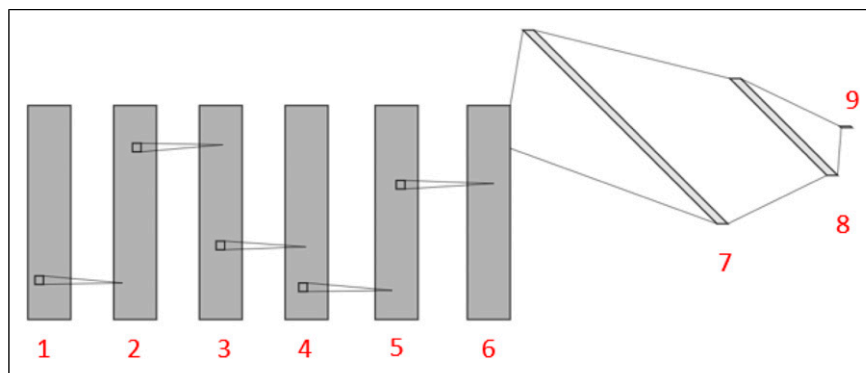


Figure 4. The Convolutional Neural Network architecture for impact location identification: 1–input layer, 2 to 6–convolution combined with max pooling layers, 7–flattened layer, 8–dense layer, 9–output layer.

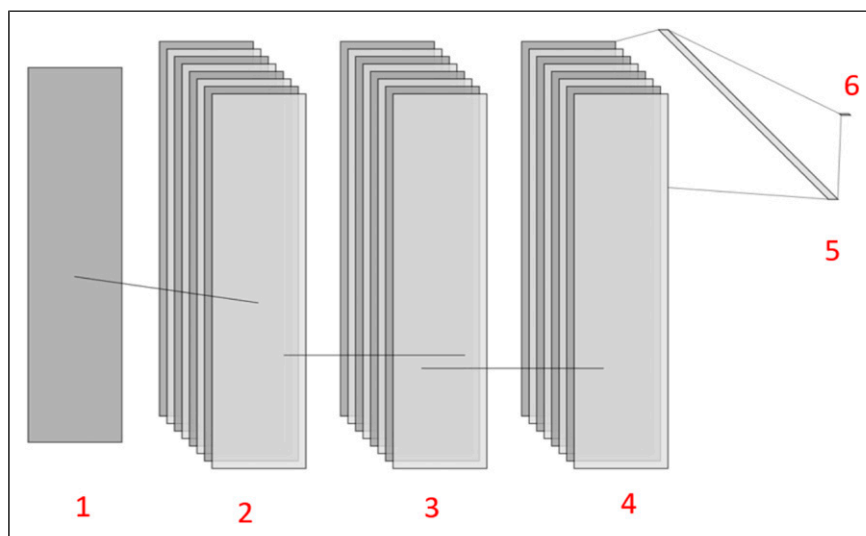


Figure 5. The LSTM architecture for the impact location identification: 1–input layer, 2 to 4–LSTM layers with 8 units, 5–flattened layer, 6–output layer.

network. The input (matrix of size 8000×1) is passed through three LSTM layers with eight units each to make a matrix of $8000 \times 8 \times 1$. The *return sequence* was turned on between the two consecutive LSTM layers to ensure effective communication. The output from the final LSTM layer is flattened and connected to the output matrix of size 2×1 .

The LSTM network was trained similarly to the previous networks by splitting the total dataset into training, validation, and testing datasets with a 70/15/15 ratio, respectively. The difference between training, validation, and testing dataset MAE was monitored to eliminate overfitting.

Robustness against added Gaussian noise

The experiment was conducted in a laboratory environment without any influence of temperature, humidity,

operational, or environmental load changes. However, the measurement from the PZT sensors will be affected by external factors such as electrical noise, temperature, humidity, environmental, and operational loads. It is of paramount importance for any SHM algorithm to perform well and be stable when external factors affect the measurement. This paper introduced environmental loads/influences by adding Gaussian noise into the PZT responses, and the corresponding effect on these three trained neural networks was studied. Gaussian noise is an acceptable approximation of aerodynamic loads, wind influence, traffic disturbances, electrical noise, and many other sources of environmental loads.^{65–67} The Gaussian noise was used to simulate operational or environmental loads/influences in the literature multiple times^{68–70} with success. The authors acknowledge that the transfer function of the PZT sensor to the structure plays a role in

modifying the environmental loads observed on the PZT response. However, a simple Gaussian noise addition was assumed to represent the environmental loads/influences in this study and the influence of transfer function is left to a future study. The Gaussian noise will be added to the measured impact response digitally. No hardware was used to introduce the noise in the impact response. The probability density function of the Gaussian noise is

$$p(x) = \frac{1}{\sqrt{2\pi}\sigma^2} e^{-\frac{(x-\mu)^2}{2\sigma^2}} \quad (4)$$

where σ is the standard deviation, μ is the mean, and x is the instance.

Typical Signal-to-Noise Ratio (SNR) observed in the measurement chain of SHM systems is around 25–50 dB.^{71,72} The SNR is defined as

$$SNR_{dB} = 20 \log_{10} \left(\frac{A_{signal}}{A_{noise}} \right) \quad (5)$$

where A_{signal} is the amplitude of the impact response and A_{noise} is the amplitude of the noise. A signal of around 2 V is expected due to the impact generated on the plate. That corresponds to the peak noise amplitude of 0.1 to 0.005 V for 26 to 52 dB of SNR, respectively. The standard deviation selected in this study for robustness analysis range from 0.001 σ (~ 0.005 V peak noise) to 0.02 σ (~ 0.1 V peak noise).

Results

Impact response and pre-processing of data

The complete impact response data from one PZT sensor due to an impact at the center of the plate is shown in Figure 6(a). Zoomed response (around the time the signal starts) from all the four PZT sensors is presented in Figure 6(b). The elastic waves reach all four PZT sensors simultaneously ($t = 1260$ microseconds) as the distance between the impact and the four PZT sensors is the same. The impact response has a frequency content up to 25,000 Hz as confirmed by the Fast Fourier Transform (FFT) of the same (see Figure 6(c)). As the impact signal was measured using a very high sample rate, downsampling needs to be done so that neural networks are not burdened with too much data while still preserving all the information from the signal. A sampling rate higher than 10 times the maximum frequency of interest is recommended for accurate re-production of amplitude, frequency, and phase in the time-domain. A factor of 30 was chosen ($30 * 25,000 * 0.0024 = 1800$, rounded to 2000) to aid the precise estimation of TOF from time-domain signal. After applying the anti-aliasing filter, the downsampling was carried out using

a predefined sub-routine⁷³ in the Python programming language. The first 2400 microseconds of data downsampled to 2000 samples per sensor were selected as the neural networks' input. A comparison between original and downsampled data (see Figure 6(d)) shows that the downsampled data accurately reproduces the original data.

Figure 6(e) displays the signal from one PZT sensor (S1) along with the estimated TOF using AIC. Figure 6(f) shows the AIC value throughout the signal and the TOF corresponds to the time at which the AIC value is minimum. In the literature, there are many methods available for TOF estimation; however, this method works well for detecting the TOF here.

Artificial Neural Network results

The training and validation loss of the ANN is plotted in Figure 7(a). The loss decreases exponentially and reaches a plateau after 2250 epochs. The validation loss is not increasing compared to training loss, thus ensuring that the model is not overfitting the data. In addition, the testing dataset loss is comparable to the validation dataset loss, which further confirms that the neural network is not overfitting the data. The weights of the neural network must be assigned randomly to break the symmetry and reach the global solution of the problem under consideration. The influence of random initial weights was studied and the random weights which gave the best results were chosen.^{54,74,75} The test dataset MAE loss was found to be 22.04 mm for the ANN model. The true and predicted location of the five randomly chosen impacts is given in Figure 7(b). Various other architectures were explored ranging from wider double hidden layers to shorter multiple hidden layers. The results of the architectures are given in Table 1. It is found that the proposed architecture, wider and shallower, gives the best results in estimating the impact location.

Convolutional Neural Network results

The CNN model was trained for 2000 epochs, and the loss (Mean Absolute Error) was found to be exponentially decreasing. The training and validation loss over the whole training period were shown in Figure 8(a). Training the CNN more than 2000 epochs reduced the training loss without affecting the validation loss. Hence, the training of CNN was stopped at 2000 epochs to eliminate overfitting. The testing dataset MAE was found to be 30.73 mm. The true and predicted location of five randomly chosen impacts using CNN is given in Figure 8(b) along with ANN results. Even though the MAE is higher than the ANN, it is essential to note that ANN was trained on extracted features after careful study and many iterations. Similar to ANN, multiple configurations of CNN were tried, and their results are given in Table 2. The CNN architecture with increasing

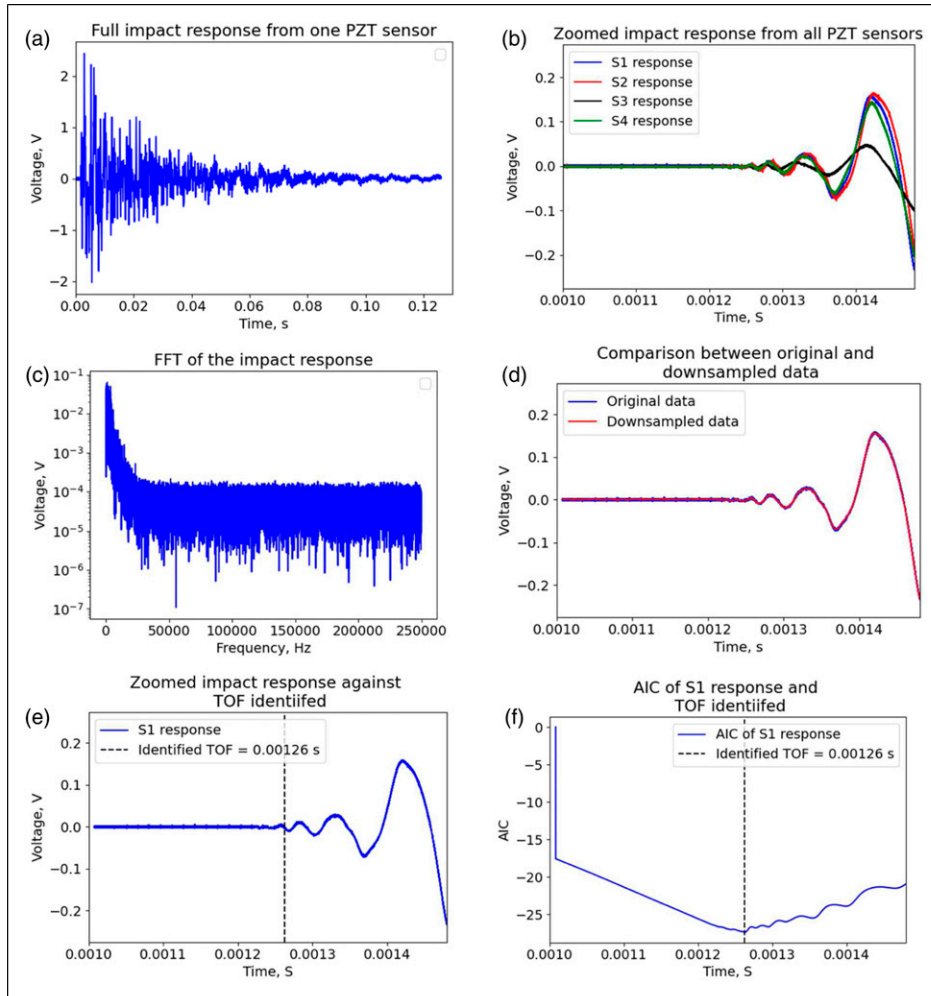


Figure 6. (a) Full impact response from one PZT sensor; (b) zoomed (around the time of signal arrival) impact response from all four PZT sensors; (c) FFT of the impact response; (d) comparison of original data with the downsampled data; (e) impact response from one PZT (S1) sensor; vertical line: TOF; and (f) AIC of the PZT response (S1) vertical line: TOF.

convolution filters from 8 to 128 performed better for the problem under consideration here.

Long Short-Term Memory network results

The network was trained for 110 epochs to ensure that the MAE loss was as minimum as possible. The training and validation loss plotted over the training cycles is given in Figure 9(a). After 110 epochs, the training and validation loss of the LSTM diverged indicating one of the characteristics of overfitting. Thus, the training of LSTM was stopped at 110 epochs. The testing dataset MAE was found to be 24.62 mm. The true and predicted locations of four randomly chosen impacts using LSTM are given in Figure 9(b), along with ANN and CNN results. The accuracy of the LSTM model is 6.11 mm higher than CNN but 2.58 mm lower than the ANN. It is important to note

that the training of the LSTM model is computationally intensive. For comparison, the LSTM model needs a couple of hours to train while the CNN and ANN need only tens of minutes on a typical personal laptop. Various architectures of LSTM were tried for the impact location identification problem and their results are presented in Table 3. The deeper LSTM model achieved maximum accuracy.

Robustness against added Gaussian noise

In this section, the stability of the neural network models under the influence of external Gaussian noise is studied quantitatively. In this regard, the dataset containing the impact responses from PZT sensors was added with Gaussian noise of increasing standard deviation (0.001, 0.002, 0.005, 0.1, and 0.2 σ). The modified PZT response

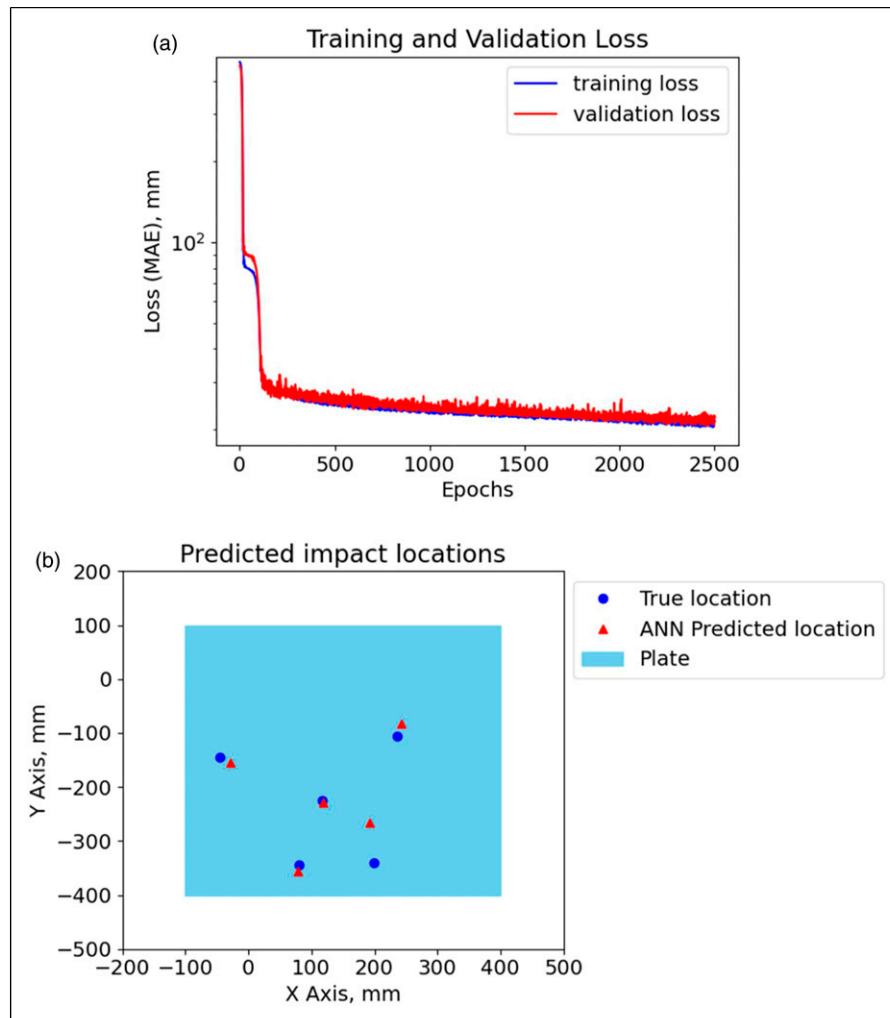


Figure 7. (a) Artificial Neural Network prediction Mean Absolute Error loss over the epochs; red: training loss, blue: validation loss and (b) true (blue dots) and predicted (red triangles) location of randomly selected five impacts.

Table I. Various architectures of Artificial Neural Network and their performances.

ANN architecture	Training	Validation	Test
Input-128-128-2	21.15	21.52	22.04
Input-32-32-32-2	26.17	29.44	27.08
Input-8-16-32-64-128-2	22.58	26.82	27.20
Input-64-64-64-2	23.74	24.28	23.12
Input-8-8-8-8-8-8-2	65.19	67.55	61.87

due to noise is presented in Figure 10. Figure 10(a) presents the laboratory-measured impact response, while Figures 10(b)–(d) present the modified PZT response due to added noise with a standard deviation of 0.001, 0.005, and 0.01, respectively. The mean of the noise was kept at 0 ($\mu = 0$) for all the noise levels. The three neural networks, developed in the earlier sections,

were tasked to predict the impact location using the noisy impact response. The MAE of each network is presented in Table 4.

The accuracy of the ANN network was affected by 11% with the maximum noise, while the CNN and LSTM's accuracies were affected only by 2% and 7%, respectively. The ANN network is the worst affected among the three. The MAE of CNN reduced slightly at a noise level of 0.005σ and increased after that. The CNN extracted features from impact responses that were not considerably affected by the added noise. This noise-tolerant feature is inherent in CNN and used in multiple domains.^{43, 49, 76}

Discussion

In terms of accuracy, the ANN is observed to be better than the other two neural networks by a good margin. The

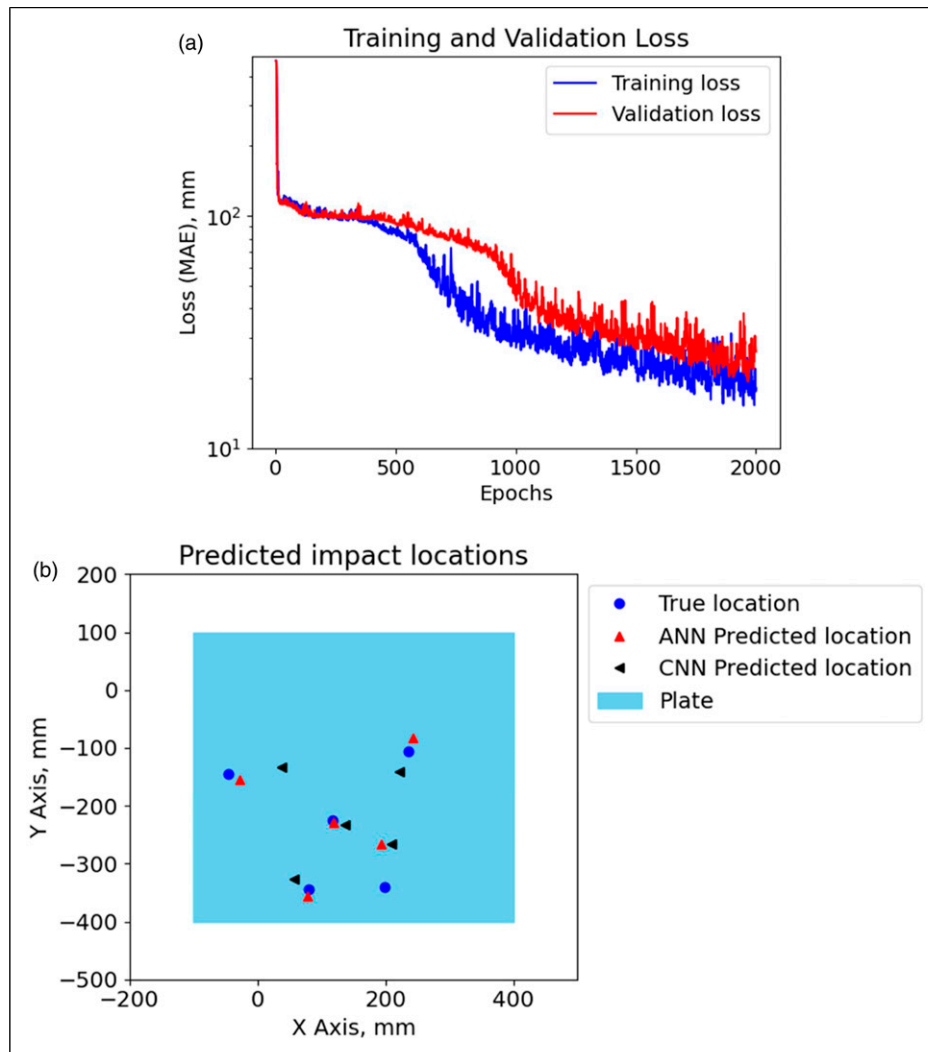


Figure 8. (a) Convolutional Neural Network prediction Mean Absolute Error loss over the epochs; red: training loss, blue: validation loss; and (b) true (blue dots) and predicted (red triangles) location of randomly selected five impacts.

Table 2. Various architectures of Convolutional Neural Network and their performances.

CNN architectures	Training	Validation	Test
Input—Convolution (filters = 8)—Max pooling—Convolution (filters = 16)—Max pooling—Convolution (filters = 32)—Max pooling—Convolution (filters = 64)—Max pooling—Convolution (filters = 128)—Flatten—Dense 128—Dense 2	30.28	29.68	30.73
Input—Convolution (filters = 8)—Max pooling—Convolution (filters = 64)—Max pooling—Convolution (filters = 64)—Max pooling—Convolution (filters = 64)—Max pooling—Convolution (filters = 64)—Flatten—Dense 128—Dense 64—Dense 2	32.30	33.5	33.12
Input—Convolution (filters = 8)—Max pooling—Convolution (filters = 8)—Max pooling—Convolution (filters = 8)—Max pooling—Convolution (filters = 8)—Max pooling—Convolution (filters = 8)—Flatten—Dense 128—Dense 64—Dense 2	32.56	34.56	36.33
Input—Convolution (filters = 8)—Max pooling—Convolution (filters = 16)—Max pooling—Convolution (filters = 16)—Max pooling—Convolution (filters = 16)—Max pooling—Convolution (filters = 16)—Flatten—Dense 128—Dense 64—Dense 2	43.33	45.46	46.87
Input—Convolution (filters = 8)—Max pooling—Convolution (filters = 16)—Max pooling—Convolution (filters = 32)—Max pooling—Convolution (filters = 64)—Max pooling—Convolution (filters = 32)—Max pooling—Convolution (filters = 16)—Flatten—Dense 128—Dense 64—Dense 2	30.11	31.23	32.10

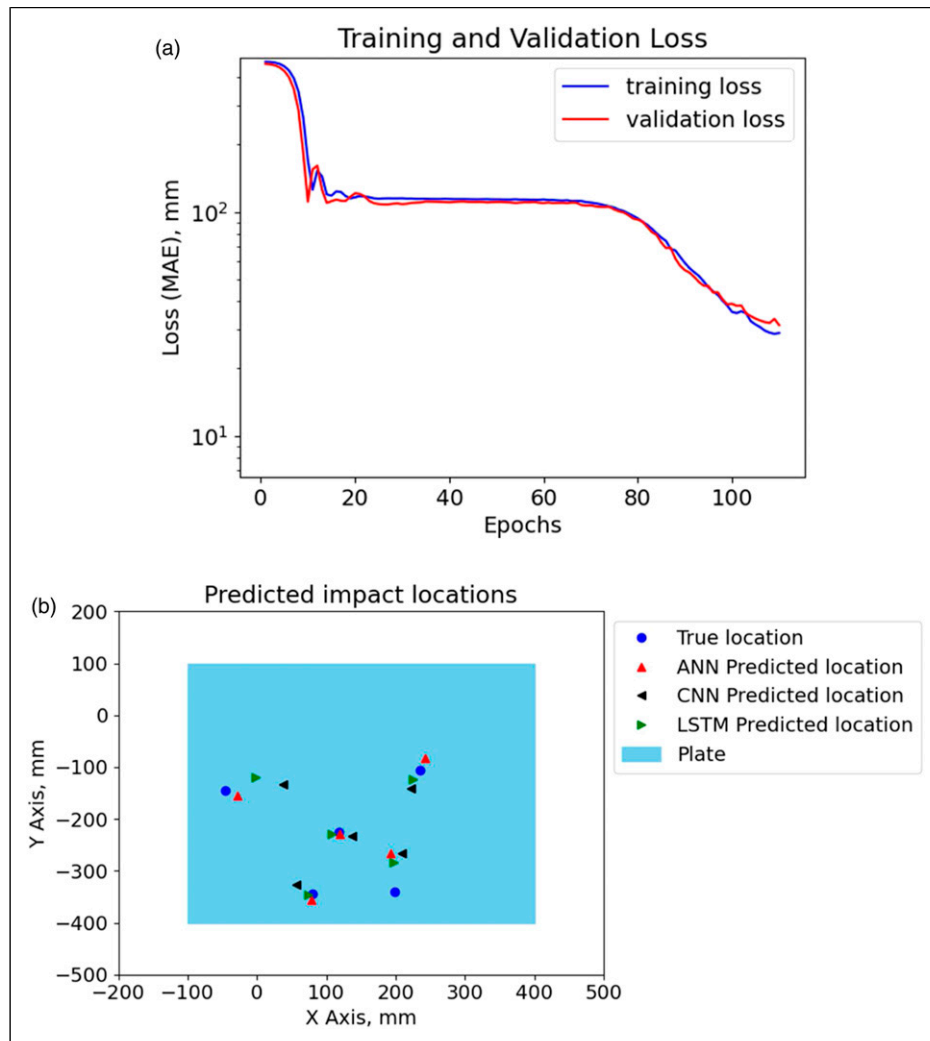


Figure 9. (a) Long Short-Term Memory network prediction Mean Absolute Error loss over the epochs; red: training loss, blue: validation loss; and (b) true (blue dots) and predicted (red triangles) location of randomly selected five impacts.

Table 3. Various architectures of Long Short-Term Memory network and their performances.

LSTM architectures	Training	Validation	Test
Input-8-8-8-2	23.04	23.87	24.62
Input-8-8-2	22.55	27.39	28.25
Input-8-16-2	32.19	31.26	33.67
Input-8-4-4-2	38.88	40.05	41.27
Input-8-4-2	25.67	25.98	30.85

accuracy of the proposed ANN is compared with the literature in Table 5. It can be seen that the accuracy of the ANN developed in this work is comparable to most of the ANNs developed earlier by other authors. However, it is essential to note that the feature extraction process must be tailored for the specific problem to achieve high accuracy.

The feature extraction process involves careful selection of the algorithm, which produces accurate features using the data available. Therefore, the feature extraction process is always affected by unforeseen external loads/influences, as seen in Table 4.

CNN performed much better than the other two neural networks in terms of robustness. The accuracy of the CNN is reduced only by 2% when it encounters the maximum noise applied in this study. LSTM follows CNN performance with a 7% accuracy reduction. The ANN suffered the most in the presence of unknown external noise. The decline in accuracy of ANN is because the added Gaussian noise influenced the extracted features. For example, the TOF identified by the AIC criterion with and without noise is given in Figure 11. The TOF estimated for the response without and with noise is 1260 and 1350 microseconds, respectively. The TOF changed about 7% when a noise with

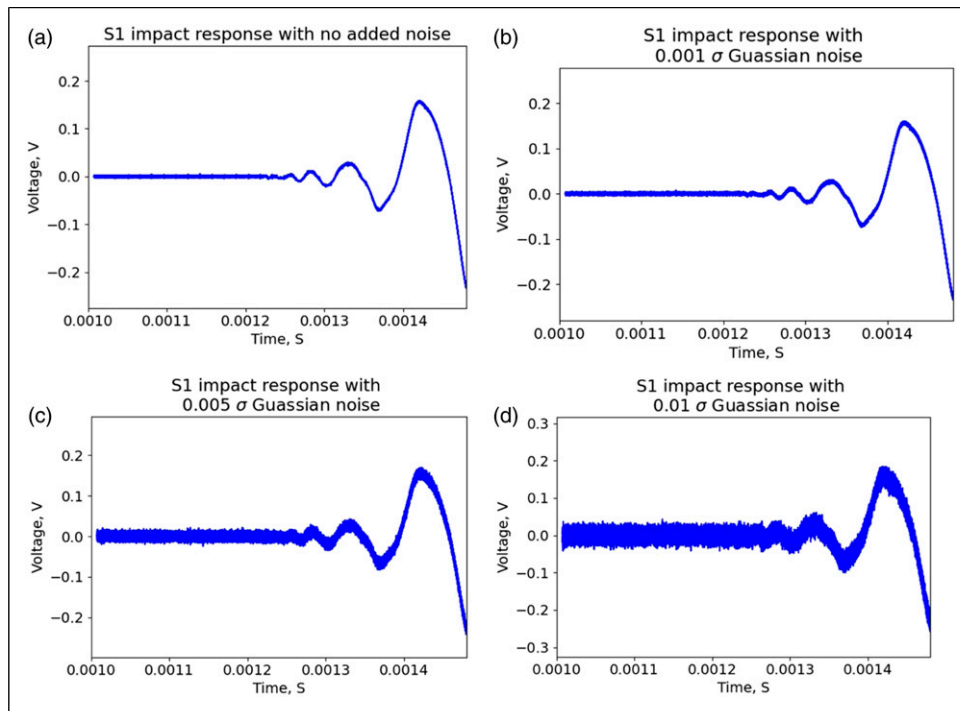


Figure 10. Addition of Gaussian noise: (a) the original signal; (b) 0.001σ Gaussian noise; (c) 0.005σ Gaussian noise; and (d) 0.01σ Gaussian noise.

Table 4. Comparison of performances of three neural networks versus Gaussian noise.

Noise level, σ	Mean Absolute Error, mm		
	ANN	CNN	LSTM
0.0	22.04	30.73	24.62
0.001	22.31	30.88	24.70
0.002	22.69	31.04	25.43
0.005	23.62	30.73	25.68
0.01	23.70	31.06	26.07
0.02	24.44	31.39	26.23

a standard deviation of 0.01 was added. The TOF change against added noise is verified on all sensors, and the percentage of average change is about 14%. This change in TOF estimation affects the overall accuracy of the ANN. It is important to note that if there are any unknown influences in the measured data, it is difficult to incorporate that in the feature extraction process. Thus, it reduced the overall accuracy of the ANN, which was trained on the dataset without noise.

The maximum frequency content of the impact response is below 25 kHz (see Figure 6(c)). The effect of applying a tight bandpass filter around the dominant frequency range is studied in this paragraph. For this purpose, a fifth-order Butterworth bandpass filter (100 Hz kHz)

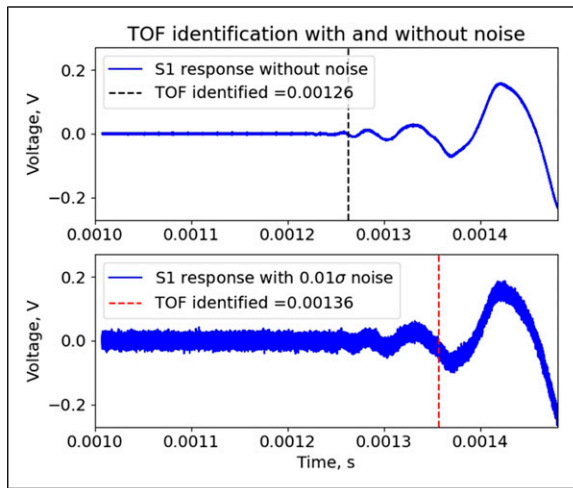
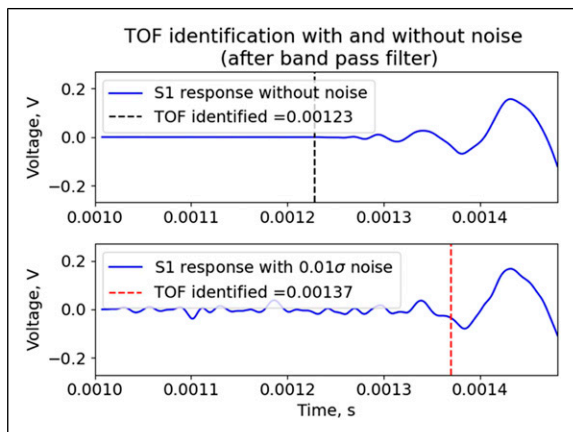
was developed using the inbuilt sub-routines⁷³ in the Python language. Figure 12 shows the result of impact response after applying bandpass filter both in the original data and the original data with 0.01σ Gaussian noise. The TOF identified by AIC was 1230 and 1370 microseconds for the response without and with noise, respectively. Like the study without a bandpass filter, there is an 11% difference in the identified TOF. The neural networks were trained as before, and the result due to added noise is given in Table 6.

It can be understood from Table 6 that the bandpass filter essentially improves the overall accuracy of all the neural networks. Nevertheless, the trend of CNN and LSTM performing better with unknown noise is evident.

From the results, it can be concluded that the CNN network is the most stable among the three and is followed by LSTM. Both CNN and LSTM are featureless neural networks, while ANN is a feature-based neural network. The feature-based neural networks will always be affected by unforeseen environmental loads/influences as shown in Table 4 and Figure 11. The high-dimensional features learnt by featureless neural networks are tolerant of unforeseen influences as supported by Table 5 and Table 6. This noise-tolerant feature of CNN is used in other areas of engineering as well.^{43,49,76} In addition to the accuracy and stability, neural networks should be computationally inexpensive to train and implement using commercial

Table 5. Comparison of performances of Artificial Neural Networks.

	MAE, mm	No. of sensors	Structure's dimension, mm
This work	22.04	4	500 × 500
¹⁸	24.40	4	530 × 300
¹⁹	38.95	9	1000 × 710
²²	45.05	4	490 × 390
²³	45.40	6	690 × 690

**Figure 11.** Effect of noise on TOF estimation: top: no noise, bottom: 0.01σ Gaussian noise.**Figure 12.** Effect of noise on TOF estimation after bandpass filter: top: no noise, bottom: 0.01σ Gaussian noise.

electronic components. It is important to note that LSTM networks are computationally expensive to train compared to the other two networks. For example, the LSTM network proposed here took a couple of hours to train while the others took tens of minutes. Because of all these results, it is the authors' opinion that CNNs are better suited for impact location identification. The effectiveness

Table 6. Comparison of performances of three neural networks versus Gaussian noise (along with bandpass filter).

	Mean Absolute Error, mm		
Noise level, σ	ANN	CNN	LSTM
0.0	21.26	30.11	23.69
0.001	21.75	30.19	23.88
0.002	21.68	30.06	24.01
0.005	23.19	30.24	24.20
0.01	23.83	30.46	24.46
0.02	24.26	30.58	24.92

and robustness of CNNs in damage classification and localization are left for a future study.

Conclusions

Structural health monitoring systems should provide the highest accuracy and robustness possible in predicting the structure's health using minimum capital investment. Characterization of impact is useful in assessing the intensity of the impact and subsequently re-evaluating the present health of the structure under monitoring with better confidence. Three of the widely used neural networks, namely Artificial Neural Network (ANN), Convolutional Neural Network (CNN), and Long Short-Term Memory (LSTM) network, were compared for their accuracy in estimating impact location from the PZT sensor response. It is found that the ANN gives better accuracy with an MAE of 22 mm, in comparison to CNN (MAE = 31 mm) and LSTM (MAE = 25 mm). Wider and shallower ANNs perform better than shorter and deeper ANNs. However, CNN was found to be more robust when encountering noise with a 2% reduction in accuracy, while LSTM and ANN lost 7% and 11% of their accuracy, respectively. Applying a bandpass filter around the frequency content of the impact response generally improves the accuracy of all three neural networks. However, the general trend of accuracy reduction due to unforeseen noise remains the same. Based on the results obtained in this study, featureless neural network CNN is suggested when robustness and ease of training are of primary concern. Another featureless neural network LSTM is suggested when moderate robustness and accuracy

are acceptable. Finally, ANN is recommended if the accuracy of foremost importance and environmental loads/influence is not expected. A similar study considering the influence of transfer function of the PZT structure and anisotropic structures is planned for future studies.

Declaration of conflicting interests

The author(s) declared no potential conflicts of interest with respect to the research, authorship, and/or publication of this article.

Funding

The author(s) received no financial support for the research, authorship, and/or publication of this article.

ORCID iD

Prabakaran Balasubramanian  <https://orcid.org/0000-0003-1602-5520>

References

1. Reveley MS, Briggs JL, Evans JK, et al. *Causal factors and adverse conditions of aviation accidents and incidents related to integrated resilient aircraft control*. NASA <https://ntrs.nasa.gov/api/citations/20100040414/downloads/20100040414.pdf>.
2. Lin B, Gresil M, Giurgiutiu V, et al. Structural health monitoring with piezoelectric wafer active sensors exposed to irradiation effects. In: Pressure Vessels and Piping Conference 2012. American Society of Mechanical Engineers.
3. Ettouney M and Alampalli S. *Infrastructure health in civil engineering*. Boca Raton, FL: CRC press, 2012.
4. Arritt BJ, Robertson LM, Henderson BK, et al. Structural health monitoring: an enabler for responsive satellites. In: *Health monitoring of structural and biological systems 2008*. International Society for Optics and Photonics, SPIE <https://www.spiedigitallibrary.org/conference-proceedings-of-spie/6935/693513/Structural-health-monitoring-an-enabler-for-responsive-satellites/10.1117/12.776336.full>
5. Richards WL, Madaras EI, Prosser WH, et al. NASA applications of structural health monitoring technology. In: International Workshop on Structural Health Monitoring NASA Presentation <https://ntrs.nasa.gov/api/citations/20140010525/downloads/20140010525.pdf>
6. Farrar CR and Worden K. An introduction to structural health monitoring. *Philosophical Trans R Soc A: Math Phys Eng Sci* 2007; 365: 303–315.
7. Farrar CR and Worden K. Structural health monitoring: a machine learning perspective. *Struct Health Monit A Machine Learn Perspective*. 2012.
8. Sohn H, Farrar CR, Hemez FM, et al. A review of structural health monitoring literature: 1996–2001. *Los Alamos Natl Lab USA* 2003; 1.
9. <https://onlinelibrary.wiley.com/doi/book/10.1002/9780470612071>
10. Ostachowicz W and Güemes A. *New trends in structural health monitoring*. Springer Science & Business Media, <https://link.springer.com/book/10.1007/978-3-7091-1390-5>
11. Qing X, Yuan S and Wu Z. Current aerospace applications of structural health monitoring in China. In: 6th European Workshop on Structural Health Monitoring, Dresden, Germany, 2012, pp.1064–1072.
12. Van Buren K, Reilly J, Neal K, et al. Guaranteeing robustness of structural condition monitoring to environmental variability. *J Sound Vibration* 2017; 386: 134–148.
13. Roach DP and Neidigk S. *Does the Maturity of Structural Health Monitoring Technology Match User Readiness?* Albuquerque, NM (United States): Sandia National Lab.(SNL-NM), 2011.
14. Malekloo A, Ozer E, AlHamaydeh M, et al. Machine learning and structural health monitoring overview with emerging technology and high-dimensional data source highlights. *Struct Health Monit* 2021; 1–50.
15. Flah M, Nunez I, Ben Chaabene W, et al. Machine learning algorithms in civil structural health monitoring: a systematic review. *Arch Comput Methods Eng*. Springer Science+Business Media B.V. 2020.
16. Giurgiutiu V. Structural health monitoring (SHM) of aerospace composites. *Polym Composites Aerospace Industry* 2019: 491–558.
17. Toh G and Park J. Review of vibration-based structural health monitoring using deep learning. *Appl Sci*. MDPI AG 2020.
18. Goodfellow I, Bengio Y and Courville A. *Deep learning*. MIT press, <https://mitpress.mit.edu/books/deep-learning>.
19. Bengio Y, Lecun Y and Hinton G. Deep learning for AI. *Commun ACM* 2021; 64: 58–65.
20. Boger Z and Guterman H. Knowledge extraction from artificial neural network models. In: 1997 IEEE International Conference on Systems, Man, and Cybernetics Computational Cybernetics and Simulation. IEEE, pp.3030–3035.
21. Alom MZ, Taha TM, Yakopcic C, et al. The history began from alexnet: A comprehensive survey on deep learning approaches. arXiv preprint arXiv:180301164 2018.
22. Hochreiter S, Bengio Y, Frasconi P, et al. Gradient flow in recurrent nets: the difficulty of learning long-term dependencies. In: *A field guide to dynamical recurrent neural networks*. IEEE Press, <https://ieeexplore.ieee.org/document/5264952>
23. Greff K, Srivastava RK, Koutník J, et al. LSTM: a search space odyssey. *IEEE Transactions Neural Networks Learning Systems* 2016; 28: 2222–2232.
24. Sonoda S and Murata N. Neural network with unbounded activation functions is universal approximator. *Appl Comput Harmonic Anal* 2017; 43: 233–268.
25. Cybenko G. Approximation by superpositions of a sigmoidal function. *Mathematics Control, Signals Systems* 1989; 2: 303–314.
26. Gomes GF, Mendez YAD, Alexandrino PdSL, et al. A review of vibration based inverse methods for damage detection and

- identification in mechanical structures using optimization algorithms and ANN. *Arch Computational Methods Engineering* 2019; 26: 883–897.
27. Min J, Park S, Yun C-B, et al. Impedance-based structural health monitoring incorporating neural network technique for identification of damage type and severity. *Eng Structures* 2012; 39: 210–220.
 28. Farhangdoust S, Tashakori S, Baghalian A, et al. Prediction of damage location in composite plates using artificial neural network modeling. In: *Sensors and Smart Structures Technologies for Civil, Mechanical, and Aerospace Systems 2019*. International Society for Optics and Photonics, p.1097001.
 29. Crivelli D, Guagliano M, Eaton M, et al. Localisation and identification of fatigue matrix cracking and delamination in a carbon fibre panel by acoustic emission. *Composites Part B: Eng* 2015; 74: 1–12.
 30. Maseras-Gutierrez M, Staszewski WJ, Found MS, et al. Detection of impacts in composite materials using piezoceramic sensors and neural networks. In: *Smart structures and materials 1998: smart structures and integrated systems*. International Society for Optics and Photonics, 1998, pp. 4 <https://www.spiedigitallibrary.org/conference-proceedings-of-spie/3329/0000/Detection-of-impacts-in-composite-materials-using-piezoceramic-sensors-and/10.1117/12.316918.full>
 31. Worden K and Staszewski WJ. Impact location and quantification on a composite panel using neural networks and a genetic algorithm. *Strain* 2000; 61–68.
 32. LeClerc J, Worden K, Staszewski WJ, et al. Impact detection in an aircraft composite panel—A neural-network approach. *J Sound Vibration* 2007; 299: 672–682.
 33. Park SO, Jang BW, Lee YG, et al. Detection of impact location for composite stiffened panel using FBG sensors. *Adv Mater Res* 2010; 895–898.
 34. Hossain MS, Ong ZC, Ng S-C, et al. Inverse identification of impact locations using multilayer perceptron with effective time-domain feature. *Inverse Probl Sci Eng* 2018; 26: 443–461.
 35. Xu Q. Impact detection and location for a plate structure using least squares support vector machines. *Struct Health Monit* 2014; 13: 5–18.
 36. Jang BW, Lee YG, Kim JH, et al. Real-time impact identification algorithm for composite structures using fiber Bragg grating sensors. *Struct Control Health Monit* 2012; 19: 580–591.
 37. Ciregan D, Meier U and Schmidhuber J. Multi-column deep neural networks for image classification. In: *2012 IEEE conference on computer vision and pattern recognition 2012*. IEEE, pp. 3642–3649.
 38. Krizhevsky A, Sutskever I and Hinton GE. Imagenet classification with deep convolutional neural networks. *Adv Neural Information Processing Systems* 2012; 25: 1097–1105.
 39. Gu J, Wang Z, Kuen J, et al. Recent advances in convolutional neural networks. *Pattern Recognition* 2018; 77: 354–377.
 40. Ronao CA and Cho S-B. Human activity recognition with smartphone sensors using deep learning neural networks. *Expert Systems Applications* 2016; 59: 235–244.
 41. Kiranyaz S, Ince T and Gabbouj M. Real-time patient-specific ECG classification by 1-D convolutional neural networks. *IEEE Trans Biomed Eng* 2015; 63: 664–675.
 42. Ince T, Kiranyaz S, Eren L, et al. Real-time motor fault detection by 1-D convolutional neural networks. *IEEE Trans Ind Electronics* 2016; 63: 7067–7075.
 43. Zhao B, Lu H, Chen S, et al. Convolutional neural networks for time series classification. *J Syst Eng Electronics* 2017; 28: 162–169.
 44. Abdeljaber O, Avci O, Kiranyaz S, et al. Real-time vibration-based structural damage detection using one-dimensional convolutional neural networks. *J Sound Vibration* 2017; 388: 154–170.
 45. Reddy A, Indragandhi V, Ravi L, et al. Detection of Cracks and damage in wind turbine blades using artificial intelligence-based image analytics. *Measurement* 2019; 147: 106823.
 46. Tabian I, Fu H and Khodaei ZS. A convolutional neural network for impact detection and characterization of complex composite structures. *Sensors (Switzerland)* 2019; 1–25.
 47. Gulgec NS, Takáč M and Pakzad SN. Convolutional neural network approach for robust structural damage detection and localization. *J Comput Civil Eng* 2019; 04019005.
 48. Chen F-C and Jahanshahi MR. NB-CNN: deep learning-based crack detection using convolutional neural network and Naïve Bayes data fusion. *IEEE Trans Ind Electronics* 2017; 65: 4392–4400.
 49. Lin M, Guo S, He S, et al. Structure health monitoring of a composite wing based on flight load and strain data using deep learning method. *Compos Structures* 2022; 115305.
 50. Sony S, Dunphy K, Sadhu A, et al. A systematic review of convolutional neural network-based structural condition assessment techniques. *Eng Structures* 2021; 226: 111347.
 51. Zargar SA and Yuan F-G. Impact diagnosis in stiffened structural panels using a deep learning approach. *Struct Health Monit* 2021; 20: 681–691.
 52. Luo H, Huang M and Zhou Z. A dual-tree complex wavelet enhanced convolutional LSTM neural network for structural health monitoring of automotive suspension. *Measurement* 2019; 137: 14–27.
 53. Bakhary N, Hao H and Deeks AJ. Damage detection using artificial neural network with consideration of uncertainties. *Eng Structures* 2007; 29: 2806–2815.
 54. Seno AH and Aliabadi M. Impact localisation in composite plates of different stiffness impactors under simulated environmental and operational conditions. *Sensors* 2019; 19: 3659.
 55. Zhang T, Biswal S and Wang Y. SHMnet: Condition assessment of bolted connection with beyond human-level performance. *Struct Health Monit* 2020; 19: 1188–1201.
 56. Hecht-Nielsen R. Theory of the backpropagation neural network. *Neural Networks for Perception* 1992; 65–93.

57. Schmidhuber J. Deep learning in neural networks: an overview. *Neural Networks* 2015; 61: 85–117.
58. Sakamoto Y, Ishiguro M and Kitagawa G. *Akaike information criterion statistics*. Dordrecht, The Netherlands: D Reidel, 1986.
59. Cavanaugh JE and Neath AA. The Akaike information criterion: Background, derivation, properties, application, interpretation, and refinements. *Wiley Interdiscip Rev Comput Stat* 2019; 11: e1460.
60. De Simone ME, Ciampa F, Boccardi S, et al. Impact source localisation in aerospace composite structures. *Smart Mater Structures* 2017; 26: 125026.
61. LeNail A. Publication-ready nn-architecture schematics, 2020 <https://alexlenail.me/NN-SVG/>.
62. Kingma DP and Ba J. Adam: a method for stochastic optimization. arXiv preprint arXiv:1412.6980 2014.
63. Aghdam HH and Heravi EJ. *Guide to convolutional neural networks*. New York, NY: Springer, 2017.
64. Géron A. *Hands-on machine learning with Scikit-Learn, Keras, and TensorFlow: Concepts, tools, and techniques to build intelligent systems*. O'Reilly Media, <https://www.oreilly.com/library/view/hands-on-machine-learning/9781492032632/>
65. Raveh DE. Identification of computational-fluid-dynamics based unsteady aerodynamic models for aeroelastic analysis. *J Aircraft* 2004; 41: 620–632.
66. Ditlevsen O. Traffic loads on large bridges modeled as white-noise fields. *J Engineering Mechanics* 1994; 120: 681–694.
67. Xu J and Tsui BM. Electronic noise modeling in statistical iterative reconstruction. *IEEE Trans Image Process* 2009; 18: 1228–1238.
68. Fan G, Li J and Hao H. Dynamic response reconstruction for structural health monitoring using densely connected convolutional networks. *Struct Health Monit* 2021; 20: 1373–1391.
69. de Castro BA, Baptista FG and Ciampa F. Comparative analysis of signal processing techniques for impedance-based SHM applications in noisy environments. *Mech Syst Signal Process* 2019; 126: 326–340.
70. Memmolo V, Ricci F, Maio L, et al. Model assisted probability of detection for a guided waves based SHM technique. *Health Monit Struct Biol Syst* 2016; 38–49.
71. Flynn EB and Todd MD. A Bayesian approach to optimal sensor placement for structural health monitoring with application to active sensing. *Mech Syst Signal Process* 2010; 24: 891–903.
72. Campeiro LM, da Silveira RZ and Baptista FG. Impedance-based damage detection under noise and vibration effects. *Struct Health Monit* 2018; 17: 654–667.
73. Virtanen P, Gommers R, Oliphant TE, et al. SciPy 1.0: fundamental algorithms for scientific computing in Python. *Nat Methods* 2020; 17: 261–272.
74. Verikas A and Bacauskiene M. Feature selection with neural networks. *Pattern Recognition Letters* 2002; 23: 1323–1335.
75. Seno AH, Khodaei ZS and Aliabadi MF. Passive sensing method for impact localisation in composite plates under simulated environmental and operational conditions. *Mech Syst Signal Process* 2019; 129: 20–36.
76. Ohtsuji T, Takeuchi T, Soma T, et al. Noise-tolerant, deep-learning-based radio identification with logarithmic power spectrum. In: ICC 2019-2019 IEEE International Conference on Communications (ICC). IEEE, pp. 1–6.